Eur. Phys. J. D (2014) 68: 98
DOI: 10.1140/epjd/e2014-50009-7

THE EUROPEAN PHYSICAL JOURNAL D

Regular Article

Infrared light extinction by charged dielectric core-coat particles

Elena Thiessen, Rafael L. Heinisch, Franz X. Bronold[a], and Holger Fehske

Institut für Physik, Ernst-Moritz-Arndt-Universität Greifswald, 17489 Greifswald, Germany

Received 3 January 2014 / Received in final form 22 February 2014
Published online 24 April 2014 – © EDP Sciences, Società Italiana di Fisica, Springer-Verlag 2014

Abstract. We study the effect of surplus electrons on the infrared extinction of dielectric particles with a core-coat structure and propose to use it for an optical measurement of the particle charge in a dusty plasma. The particles consist of an inner core with negative and an outer coat with positive electron affinity. Both the core and the coat give rise to strong transverse optical phonon resonances, leading to anomalous light scattering in the infrared. Due to the radial profile of the electron affinity electrons accumulate in the coat region making the infrared extinction of this type of particles very charge-sensitive, in particular, the extinction due to a resonance arising solely due to the core-coat structure. The maximum of this resonance is in the far-infrared and responds to particle charges realizable in ordinary dusty laboratory plasmas.

1 Introduction

More often than not contain ionized gas environments dust particles of various chemical composition and various size distribution [1,2]. For instance, astrophysical plasmas in the interstellar medium [3,4] or in the planetary magnetosphere [5] are loaded with dust particles as is the upper part of the earth atmosphere [6]. Man-made plasmas also contain dust particles, as unavoidable contaminations of industrial processing discharges [7], as the desired product of a particle synthesis [8], or simply as a physical subsystem whose self-organization and feedback to the hosting plasma is the object of scientific inquiry [9].

The most important effect a dust particle has on a plasma environment is the collection of electrons. A dust particle is thus a sink for the species most important for sustaining the plasma and knowing the charge accumulated by the particle is of great interest. It has been measured in a number of experiments [10–18]. Most methods depend on a force balance and hence on the plasma parameters at the position of the particle. Usually, however, not even the electric force is known precisely, let alone the various viscous forces resulting in large uncertainties of the measured particle charge. More sophisticated methods have been developed, for instance, the phase-resolved resonance method by Carstensen et al. [18], but for an absolute charge measurement they also require plasma parameters. Despite all the efforts over more then two decades measuring the charge of a dust particle in a dusty plasma remains an experimental challenge [14].

To overcome the limitations of the traditional methods of measuring the particle charge we started an investigation of the interaction of light with charged micron- and submicron-sized dielectric particles looking in particular for distortions in the Mie extinction signal due to the charge of the particle [19,20]. That the scattering of light by small particles (Mie scattering [21–23]) encodes, at least in principle, the particle charge is well-known [23–28]. Rosenberg [29] also pointed out that Mie scattering by the dust particles in a dusty plasma may provide access to the particle charge. Systematic calculations are however required to determine the type of particles which show particularly strong charge-induced modifications of the Mie signal and are hence most suitable for an optical charge diagnostics.

In our previous work we found the maximum of the anomalous infrared extinction of a particular class of dielectric particles to depend on the particle charge [19,20]. Initially, Tribelsky and Luk'yanchuk [30,31] identified this type of extinction in a theoretical study of the interaction of light with small metallic particles. Quite generally, anomalous extinction arises in the spectral region where the real part of the particle's dielectric function crosses minus two while the imaginary part stays very small. For metallic particles this happens above the plasmon frequency and hence in the optical part of the spectrum. Dielectric particles having strong transverse optical phonon resonances in the dielectric function, for instance, Al_2O_3, CaO or LiF, also show this type of resonance. It appears in the infrared and turns out to be charge-sensitive. Using particles showing anomalous extinction in dusty plasmas may thus open the door to measure the particle charge optically by a simple infrared attenuation experiment.

The set-up of such an experiment is sketched in Figure 1. It is similar to the one routinely used in other kinds of in-sito infrared plasma diagnostics [32]. The particle charge would reveal itself by the position of the extinction maximum. No information about the plasma would be required. In Figure 2 we show the expected extinction efficiency for a homogeneous Al_2O_3 particle with radius $a = 0.1$ μm as obtained from our previous

[a] e-mail: bronold@physik.uni-greifswald.de

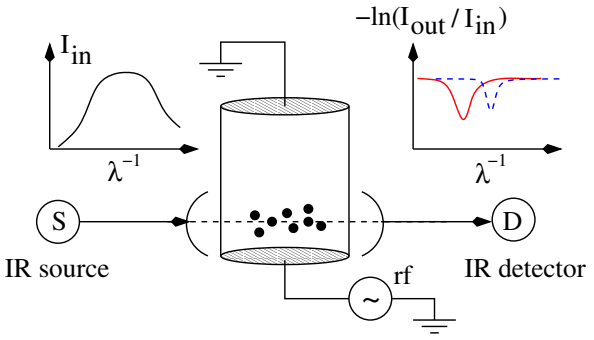

Fig. 1. Experimental set-up for an optical measurement of the particle charge in a dusty plasma using anomalous infrared extinction. The detected outgoing light intensity $I_{\rm out}(\lambda^{-1}) = I_{\rm in}(\lambda^{-1})\exp[-\pi a^2 l_{\rm opt} n_{\rm d} Q_{\rm t}(\lambda^{-1})]$ with $I_{\rm in}(\lambda^{-1})$ the intensity of the incoming light with wave length λ, a the particle radius, $l_{\rm opt}$ the length of the optical path, $n_{\rm d}$ the dust density, and $Q_{\rm t}(\lambda^{-1})$ the extinction efficiency. The position of the extinction maximum depends on the charge and can thus be used for its determination.

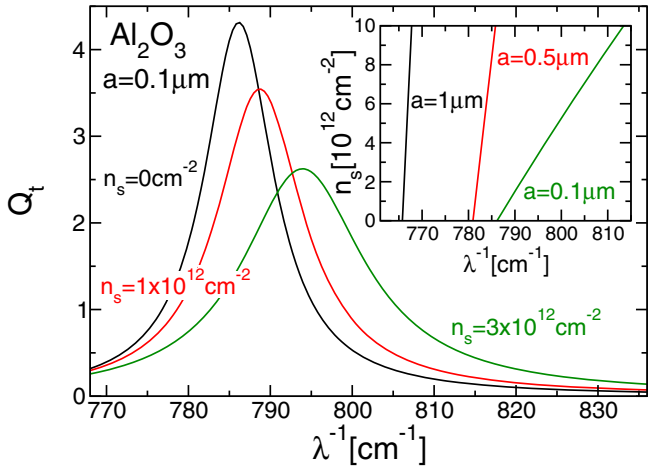

Fig. 2. Extinction efficiency Q_t due to the anomalous vibron resonance as a function of the inverse wave length for a homogeneous Al_2O_3 particle with radius $a = 0.1$ μm and various surface charge densities n_s. Inset: position of the extinction maximum due to the anomalous vibron resonance as a function of n_s for different particle radii. The larger the radius the weaker the shift of the extinction maximum.

investigations [20]. The shift of the extinction maximum as a function of the surface charge density can be clearly seen. To produce a shift of one wave number the particle has to charge up to $Z_p = Q_p/(-e) \approx 5 \times 10^2$ which seems to be not too far away from the charge a particle of this size would acquire in an ordinary dusty plasma experiment [16]. The charge-induced shift decreases however strongly with particle size (see inset). A micron-sized particle, for instance, would have to charge up to $Z_p \approx 6 \times 10^5$ to induce a shift of one wave number. In reality, however, leaving specialized plasmas containing high-energy electrons aside [33,34], a micron-sized particle carries most probably much less charge [16]. It looks like as if the proposed optical charge diagnostics is only feasible for rather small particles.

The purpose of the present work is to describe a possibility to optimize the charge-induced shift of the extinction maximum. Below we show that particles with a core-coat structure substantially improve the perspectives of an optical charge measurement. The idea is to insert a dielectric core with negative electron affinity inside a dielectric particle with positive electron affinity. For instance, a CaO core inside an Al_2O_3 particle. Both materials give rise to anomalous extinction. Instead of one two extinction resonances at different wave numbers may now be used for the charge diagnostics. The added flexibility is however not what makes this type of inhomogeneous particle so attractive. More important is that due to the particular choice of the electron affinities surplus electrons collected from the plasma pile up in the coat region. The increased volume density of the surplus electrons results in an increased charge-induced shift of the extinction maximum due to the core. Surprisingly it does not much affect the charge sensitivity of the anomalous resonance of the coat although the electrons are concentrated in this region. However, the core-coat structure leads to a new resonance [35] at larger wave numbers which turns out to be particularly sensitive to the charge. The position of this resonance shifts already by one wave number at charge densities typical for particles in ordinary dusty laboratory plasmas making it thus an excellent optical probe for the particle charge.

In the next section and in the Appendix we give the theoretical background of Mie scattering by charged dielectric particles with a core-coat structure. In particular we explain how the particle charge enters the formula for the Mie extinction efficiency via the electric conductivity in the coat region. Numerical results for material combinations most suitable for an optical charge measurement are given in Section 3. In Section 4 we summarize the main points and discuss experimental issues which may arise when the approach is actually put into place.

2 Theoretical background

We consider the scattering of a linearly polarized electromagnetic plane wave by a small spherical particle with radius a consisting of an inner core (region 1) with radius $b = fa$, where f denotes the filling factor, and an outer coat (region 2) with thickness $d = (1 - f)a$ as schematically shown in Figure 3. A particle with such a core-coat structure we call coated particle.

The material we take for the core has negative electron affinity, for instance, CaO MgO, or LiF, while the electron affinity of the coat is positive. Due to this particular choice surplus electrons collected from the plasma cannot penetrate into the core. They accumulate in the coat and modify via their conductivity the dielectric function in this region. A core with a less positive electron affinity than the coat would also produce a potential well for the excess electrons in the coat region. But the well would be less deep. We do not discuss this possibility further but point out that electron bags could be engineered by stacking suitable materials.

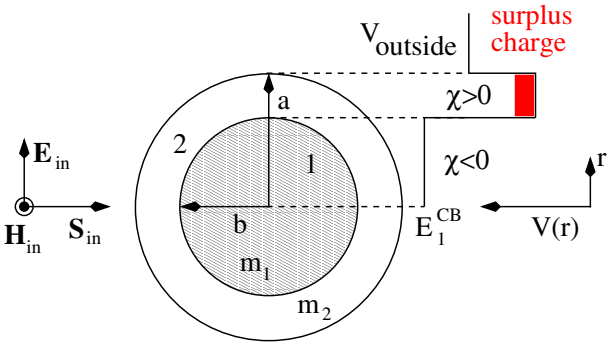

Fig. 3. Sketch of the particle design and the scattering geometry. On the left is shown the incident electromagnetic plane wave characterized by a Poynting vector $\mathbf{S}_{\rm in}$, an electric field $\mathbf{E}_{\rm in}$, and a magnetic field $\mathbf{H}_{\rm in}$. The surplus electrons are confined in the potential profile $V(r)$ shown on the right. It arises if the core (region 1) is made out of a material with negative electron affinity $\chi < 0$ while the coat (region 2) is made out of a material with positive electron affinity $\chi > 0$. The index of refraction in the two regions is $m_{1,2} = \sqrt{\varepsilon_{1,2}}$, where ε_i is the complex dielectric function in region i, including for $i = 2$ the modification due to the charge. The radius of the particle is a while the radius of the core is b. Introducing a filling factor $f = b/a$ measuring the core radius in units of the particle radius the thickness of the coat can be written as $d = (1 - f)a$.

The modification of the dielectric function of the coat due to the surplus electrons affects the electromagnetic energy the particle absorbs and scatters per unit time. Divided by the incident energy flux per unit surface and normalized to an area of a circle with radius a this quantity is called extinction efficiency [22,23] and has been worked out for a coated particle in general long time ago by Aden and Kerker [36]. The main steps of the calculation, which can be also found in the textbook by Bohren and Huffman [23], are presented in the Appendix to make our presentation self-contained. In the notation of Bohren and Huffman [23] which differs from the notation we used previously [19,20] the extinction efficiency of a coated particle reads [37]

$$Q_t = \frac{2}{y^2}\mathrm{Re}\sum_{n=1}^{\infty}(2n+1)(a_n + b_n), \tag{1}$$

where

$$a_n = C_n^{-1}\Big\{\psi_n(y)[\psi_n'(m_2y) - A_n\chi_n'(m_2y)] - m_2\psi_n'(y)[\psi_n(m_2y) - A_n\chi_n(m_2y)]\Big\}, \tag{2}$$

$$b_n = D_n^{-1}\Big\{m_2\psi_n(y)[\psi_n'(m_2y) - B_n\chi'(m_2y)] - \psi_n'(y)[\psi_n(m_2y) - B_n\chi_n(m_2y)]\Big\} \tag{3}$$

Table 1. Parameters for the materials considered in this work. The dielectric functions of the materials used for the core (CaO [38], MgO [39] and LiF [39]) and the coat (PbS [40] and Al_2O_3 [41,42]) are given by equations (18) and (19), respectively. For the two coat materials we also need the effective mass of the electron [43,44] which enters (11) for the electric conductivity.

	CaO	MgO	LiF	PbS	Al_2O_3
$\bar{\varepsilon}_\infty$	3.3856	3.01	1.9	16.81	3.2
ν_1 [cm^{-1}]	298	401	306	71	385
f_1	9	6.6	6.8	133.19	0.3
γ_1 [cm^{-1}]	32	7.619	18.36	15	5.58
ν_2 [cm^{-1}]	–	640	503	–	442
f_2	–	0.045	0.11	–	2.7
γ_2 [cm^{-1}]	–	102.4	90.54	–	4.42
ν_3 [cm^{-1}]	–	–	–	–	569
f_3	–	–	–	–	3
γ_3 [cm^{-1}]	–	–	–	–	11.38
ν_4 [cm^{-1}]	–	–	–	–	635
f_4	–	–	–	–	0.3
γ_4 [cm^{-1}]	–	–	–	–	12.7
m_e^*/m_e	–	–	–	0.175	0.4

are Mie scattering coefficients with

$$A_n = \frac{m_2\psi_n(m_2x)\psi_n'(m_1x) - m_1\psi_n'(m_2x)\psi_n(m_1x)}{m_2\chi_n(m_2x)\psi_n'(m_1x) - m_1\chi_n'(m_2x)\psi_n(m_1x)}, \tag{4}$$

$$B_n = \frac{m_2\psi_n(m_1x)\psi_n'(m_2x) - m_1\psi_n(m_2x)\psi_n'(m_1x)}{m_2\chi_n'(m_2x)\psi_n(m_1x) - m_1\psi_n'(m_1x)\chi_n(m_2x)}, \tag{5}$$

and

$$C_n = \xi_n(y)[\psi_n'(m_2y) - A_n\chi_n'(m_2y)] - m_2\xi_n'(y) \times [\psi_n(m_2y) - A_n\chi_n(m_2y)], \tag{6}$$

$$D_n = m_2\xi_n(y)[\psi_n'(m_2y) - B_n\chi_n'(m_2y)] - \xi_n'(y) \times [\psi_n(m_2y) - B_n\chi_n(m_2y)]. \tag{7}$$

Here, $x = kb$ is the size parameter of the inner core while $y = ka$ is the size parameter of the total particle, where in both cases $k = 2\pi\lambda^{-1}$, that is, the wave number multiplied by 2π. The functions ψ_n, ξ_n and χ_n are Riccati-Bessel functions as defined in Stratton's textbook [22] and $m_i = \sqrt{\varepsilon_i}$ denotes for $i = 1$ the refractive index of the core and for $i = 2$ the refractive index of the coat including the effect of surplus electrons.

The dielectric function of the uncharged particle is given by the dielectric function of the core material $\bar{\varepsilon}_1$ and the dielectric function of the coat material $\bar{\varepsilon}_2$ depending on the spatial region. We assume $\bar{\varepsilon}_1$ and $\bar{\varepsilon}_2$ to be known either in the form of a suitably parameterized set of Lorentz oscillators (see next section and Tab. 1) or in the form of tabulated experimental data. The dielectric function of the coat is modified by the surplus electrons,

$$\varepsilon_2 = \bar{\varepsilon}_2 + 4\pi i\frac{\sigma_2}{\omega}, \tag{8}$$

where σ_2 is the electric conductivity due to the surplus electrons and $\omega = kc$.

The calculation of σ_2 is based on the assumption that at quasi-stationarity surplus electrons form an interface-specific electron distribution, the electron surface layer [45], thermalized with the dust particle and bound in the potential profile $V(r)$ arising due to the radial variation of the electron affinities of the dielectric materials used for the core and the coat (see Fig. 3). Since the electron affinity of the core is negative surplus electrons pile up in the coat region, that is, they will occupy the conduction band of the coat material. The binding energy of the surplus electrons is thus on the order of the electron affinity of the coat, which, for the materials we consider, is on the order of an electron volt. If the coat had negative electron affinity surplus electrons would not enter the grain at all. Instead they would pile up in the image potential in front of the grain surface [45]. We do not consider this case below.

For the description of the conduction band states of the coat we restrict ourselves at the moment to a planar bulk model [45,46], that is, we assume surplus electrons to occupy bulk states of the dielectric and to scatter off bulk phonons. The planar bulk model is applicable if the following conditions are satisfied: first, the radius a of the particle has to be much larger than the thermal de Broglie wave length of a surplus electron inside the coat $\lambda_e^{dB} = 2\pi a_B\sqrt{R_y m_e/E_0 m_e^*}$ with m_e^* and m_e the effective and bare mass of the electron, respectively, a_B the Bohr radius, R_y the Rydberg energy, and $E_0 = \pi k_B T$ the thermal energy of the electron; T is the temperature of the particle. Second, the thickness of the coat $d = a - b = a(1 - f)$ with f the filling factor has to be such that the confinement energy of an electron in the coat $E_c = (\pi^2/2)R_y(m_e/m_e^*)(a_B/d)^2$ is much smaller than E_0. Typically, $T \simeq 300$ K leading to $E_0 \simeq 0.08$ eV and hence to $\lambda_{dB} \simeq 10$ nm. Thus, for micron-sized particles the curvature of the particle can be safely neglected. The confinement energy is more critical. It depends on the effective mass. The smaller the effective mass the larger the confinement energy. The coat materials we consider are Al_2O_3 for which $m_e^* = 0.4m_e$ and PbS for which $m_e^* = 0.175m_e$. The more restrictive material is thus PbS. Taking for instance $a = 0.05$ μm and $f = 0.9$ leads for a PbS coat to $E_c \simeq 0.04$ eV which is on the order of the thermal energy of an electron implying that quantum confinement may already play a role. To avoid complications due to quantum confinement we thus have to decrease f or increase a.

With these restrictions in mind we base the calculation of σ_2 on the bulk Hamiltonian

$$H = \sum_{\boldsymbol{k}} \varepsilon(\boldsymbol{k}) c_{\boldsymbol{k}}^\dagger c_{\boldsymbol{k}} + \hbar\omega_{\mathrm{LO}} \sum_{\boldsymbol{q}} a_{\boldsymbol{q}}^\dagger a_{\boldsymbol{q}} + \sum_{\boldsymbol{k},\boldsymbol{k}'} D(\boldsymbol{k}-\boldsymbol{k}')\left[c_{\boldsymbol{k}}^\dagger c_{\boldsymbol{k}'} a_{\boldsymbol{k}-\boldsymbol{k}'} + h.c.\right], \quad (9)$$

where, within the effective mass approximation, $\varepsilon(\boldsymbol{k}) = \hbar^2\boldsymbol{k}^2/2m_e^*$ is the energy of a surplus electron in the coat region measured from the bottom of the conduction band,

$$D(\boldsymbol{k}-\boldsymbol{k}') = \sqrt{\frac{2\pi e^2\hbar\omega_{\mathrm{LO}}}{V(\boldsymbol{k}-\boldsymbol{k}')^2}\left(\frac{1}{\bar{\varepsilon}_\infty} - \frac{1}{\bar{\varepsilon}_0}\right)} \quad (10)$$

is the electron-phonon coupling matrix element, and $\hbar\omega_{\mathrm{LO}}$ is the energy of the longitudinal optical (LO) bulk phonon which for simplicity we assumed to be independent of the phonon momentum $\boldsymbol{q}$. Scattering by LO phonons is the dominant scattering process in dielectrics at room temperature. Other scattering processes are therefore neglected. The operator $c_{\boldsymbol{k}}^\dagger$ creates an electron with momentum $\boldsymbol{k}$ while the operator $a_{\boldsymbol{q}}^\dagger$ creates a phonon with momentum $\boldsymbol{q}$. Within the planar bulk model all momenta are three-dimensional vectors.

Following the seminal work by Götze and Wölfle [47] we write the conductivity

$$\sigma_2(\omega) = \frac{n_{a-b}e^2}{m_e^*}\frac{i}{\omega + M(\omega)} \quad (11)$$

in terms of a memory function $M(\omega)$ which takes current-limiting scattering processes into account. In our case, the current is limited only by electron-phonon scattering. The electron density in (11), $n_{a-b} = 3Z_p/4\pi(a^3 - b^3)$ is the number of elementary charges Z_p accumulated by the particle divided by the coat volume. Treating the electron-phonon coupling in (9) in second order perturbation theory [47],

$$M(\omega) = -\frac{\bar{D}^2}{V}\sum_{\boldsymbol{k},\boldsymbol{k}'}\sum_{\boldsymbol{p},\boldsymbol{p}'}\frac{v_x(\boldsymbol{k}) - v_x(\boldsymbol{k}')}{|\boldsymbol{k}-\boldsymbol{k}'|}\frac{v_x(\boldsymbol{p}) - v_x(\boldsymbol{p}')}{|\boldsymbol{p}-\boldsymbol{p}'|} \times \left\{\left\langle\left\langle c_{\boldsymbol{k}}^\dagger c_{\boldsymbol{k}'} a_{\boldsymbol{k}-\boldsymbol{k}'}; c_{\boldsymbol{p}}^\dagger c_{\boldsymbol{p}'} a_{\boldsymbol{p}-\boldsymbol{p}'}\right\rangle\right\rangle_\omega + c.c.\right\} \quad (12)$$

with $v_x(\boldsymbol{k}) = \hbar k_x/m_e^*$ the x-component of the velocity of an electron with momentum $\boldsymbol{k}$ and

$$\bar{D} = \sqrt{2\pi e^2\hbar\omega_{\mathrm{LO}}\left(\bar{\varepsilon}_\infty^{-1} - \bar{\varepsilon}_0^{-1}\right)} \quad (13)$$

a constant. The correlation function within the curly brackets is defined by [47]:

$$\langle\langle A; B\rangle\rangle_z = -i\int_0^\infty dt e^{-izt}\langle[A(t), B(0)]\rangle \quad (14)$$

with $[A(t), B(0)]$ the commutator between operators $A(t)$ and $B(0)$ which evolve in time according to the non-interacting system, that is, according to (9) without electron-phonon coupling. The brackets under the integral (14) stand for the grand-canonical thermal average. Beyond second order perturbation theory the memory function would look differently. It would then also be necessary to calculate the correlation function with the full Hamiltonian.

After a straightforward but lengthy calculation one finds for the memory function a concise expression [20],

$$M(\omega) = \bar{M}\int_{-\infty}^{\infty} d\bar{\nu}\frac{j(-\bar{\nu}) - j(\bar{\nu})}{\bar{\nu}\,(\bar{\nu} - \nu - \mathrm{i}0^+)} \quad (15)$$

with

$$\bar{M} = \frac{4e^2\sqrt{m_e^*\omega_{\rm LO}\delta}\left(\bar{\varepsilon}_\infty^{-1} - \bar{\varepsilon}_0^{-1}\right)}{2(3\pi\hbar)^{3/2}} \tag{16}$$

a constant and

$$j(\nu) = \frac{e^\delta}{e^\delta - 1} e^{-\frac{\delta}{2}(\nu+1)} |\nu+1| K_1\left(\tfrac{\delta}{2}|\nu+1|\right) + \frac{1}{e^\delta - 1} e^{-\frac{\delta}{2}(\nu-1)} |\nu-1| K_1\left(\tfrac{\delta}{2}|\nu-1|\right) \tag{17}$$

a function defined in terms of the modified Bessel function $K_1(x)$ [48]. The parameter $\delta = \hbar\omega_{\rm LO}/k_BT$ gives the phonon energy in units of k_BT and $\nu = \omega/\omega_{\rm LO}$ is the electron energy normalized to the phonon energy.

The memory function (15) is independent of the electron density. However, due to the prefactor in (11) the electric conductivity depends linearly on the density of the surplus electrons. The higher the electron density the higher the electric conductivity in the coat and hence the larger the modification of the dielectric function (8). Since the refractive index of the coat, $m_2 = \sqrt{\varepsilon_2}$, enters the Mie scattering coefficients (2) and (3) the extinction efficiency (1) also depends on the electron density. It is this effect we propose to utilize as a charge diagnostics. From (11) it can be also deduced that the charge-induced modification of the extinction efficiency will be the larger the smaller the effective electron mass is.

In principle we could have based the calculation of the conductivity on a more sophisticated Hamiltonian taking the curvature of the particle as well as quantum confinement into account. The matrix elements defining the Hamiltonian could be worked out. However, it would then be also necessary to allow for non-locality in the optical response of the uncharged particle. Since the radii of the particles most commonly used in dusty laboratory plasmas are at least a few tenth of a micron such an improved treatment is at the moment not required.

3 Results

In the following we discuss infrared extinction for a representative selection of coated dielectric particles at room temperature. Depending on the plasma conditions, particle size, and surface properties the particle temperature could be also one hundred degree Celsius higher [49] but this would modify our results only slightly.

The dielectric functions of the materials we consider can be found in the literature. They are parameterized by a set of damped harmonic oscillators. Separating real and imaginary parts the dielectric functions can be written as [38–42]

$$\bar{\varepsilon}' = \bar{\varepsilon}_\infty + \sum_{j=1}^{2} \frac{f_j\nu_j^2\left(\nu_j^2 - \nu^2\right)}{\left(\nu_j^2 - \nu^2\right)^2 + \gamma_j^2\nu_j^2}, \tag{18}$$

$$\bar{\varepsilon}'' = \sum_{j=1}^{2} \frac{f_j\nu_j^2\gamma_j\nu}{\left(\nu_j^2 - \nu^2\right)^2 + \gamma_j^2\nu_j^2}, \tag{19}$$

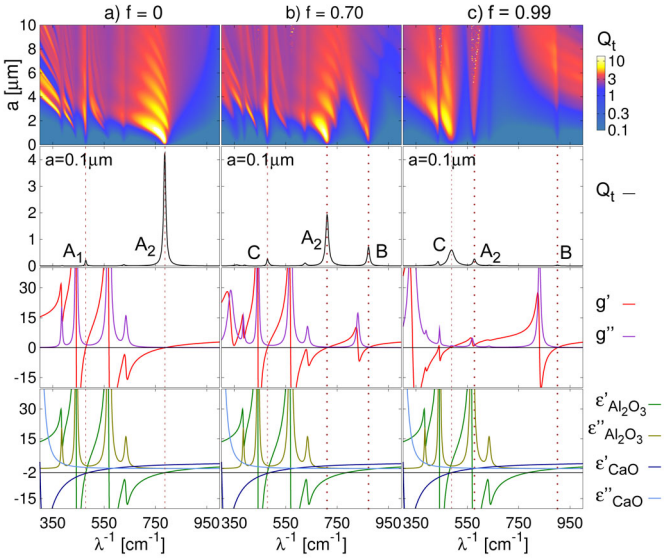

Fig. 4. Top most panel: extinction efficiency Q_t as a function of wave number λ^{-1} and particle radius a for an uncharged Al_2O_3 particle containing a CaO core with radius $b = fa$. Second top most panel: horizontal cut at $a = 0.1$ μm through the extinction efficiency plotted in the panel above showing the nomalous resonances of the coat (features A_1 and A_2), the anomalous resonance of the core (feature C), and the shell resonance (feature B). The functions g' and g'' given in the panel underneath determine the positions and the strengths of these three resonances. The panel at the bottom shows the dielectric functions of the core and the coat material separately and without surplus electrons taken into account.

where in accordance with the notation employed in (8) an overbar is used to indicate that in the dielectric functions the effect of surplus electrons is not yet taken into account. The frequencies ν_i, oscillator strengths f_i, and damping rates γ_i are given in Table 1 together with $\bar{\varepsilon}_\infty$, the value of the dielectric function at high frequencies.

Before discussing the extinction by charged coated dielectric particles it is useful to consider the extinction by uncharged particles. Thereby the spectral features potentially useful for an optical charge measurement can be identified. Let us therefore start with the two up-most panels of Figure 4 which show for three filling factors f the extinction efficiency Q_t of an uncharged CaO/Al_2O_3 particle as a function of the particle radius a and the wave number λ^{-1}. For $f = 0$ the particle is a homogeneous Al_2O_3 particle showing the expected sequence of anomalous resonances around $\lambda^{-1} \approx 490$ cm^{-1} (feature A_1) and $\lambda^{-1} \approx 786$ cm^{-1} (feature A_2) while for $f = 0.99$ the particle is essentially a homogeneous CaO particle with anomalous resonances appearing around 488 cm^{-1} (feature C). That this assignment is correct can be seen from the lowest row of the panel which shows the real and imaginary parts of the dielectric functions for CaO and Al_2O_3. The resonances appear at wave numbers where $\bar{\varepsilon}' = -2$ and $\bar{\varepsilon}'' \ll 1$ as it should be for anomalous resonances of uncharged particles (see dashed vertical lines) [19,20]. A closer look reveals that for all filling factors $0 < f < 1$ an additional

resonance (feature B) appears above the anomalous resonance of the coat material. The strength and position of this resonance, which we call shell resonance for reasons which become clear in a moment, depends on f. Specifically for $f = 0.7$ it shows up at $\lambda^{-1} \approx 872\,\mathrm{cm}^{-1}$. The three dominant features – A_2, B, and C – can be most clearly seen in the second row of the panel, where the extinction efficiency is plotted for a fixed particle radius $a = 0.1\ \mu$m.

Of particular interest is feature B. It appears at the largest wave number. Within the electrostatic approximation [35] feature B can be understood as the anti-bonding split-off of the anomalous resonance of the coat due to its mixing with a cavity mode supported by the core. If the filling factor f is sufficiently large, that is, if the coat surrounding the core is sufficiently thin, the two modes are strongly mixed resulting in a doublet whose splitting and relative spectral weights are a function of the filling factor. From panel (b) in Figure 4 it is apparent that features A_2 and B are the bonding and anti-bonding partners expected from this scenario.

The electrostatic approximation holds for small enough particles where the dipole contribution ($n = 1$) dominates the sum (1). It gives a physically very appealing picture and has the advantage that it can be also applied to particles of arbitrary shape [35]. We consider at the moment however only spherical particles and can thus employ the full Mie theory. That for sufficiently small core-coat particles an additional extinction resonance appears can be also deduced from the full expression (1) by employing an expansion similar to the one we used for homogeneous particles [19,20]. In the limit $x, y \ll 1$,

$$Q_t \simeq -\frac{6}{y^2}\frac{f' g''}{(g'')^2 + (g')^2} \tag{20}$$

with f' an almost constant function and g' and g'' the real and imaginary parts of a function g which acts as the effective dielectric function of the particle shifted by two; resonances appear therefore for $g' = 0$. Defining

$$F = \frac{2f^3}{(\varepsilon_1' + 2\varepsilon_2')^2 + (\varepsilon_1'' + 2\varepsilon_2'')^2} \tag{21}$$

the two functions are given by

$$\begin{aligned} g' = \varepsilon_2' + 2 + F\big\{&(\varepsilon_2' - 1)\big[(\varepsilon_1' - \varepsilon_2')(\varepsilon_1' + 2\varepsilon_2') \\ &+ (\varepsilon_1'' - \varepsilon_2'')(\varepsilon_1'' + 2\varepsilon_2'')\big] + \varepsilon_2''\big[(\varepsilon_1' - \varepsilon_2')(\varepsilon_1'' + 2\varepsilon_2'') \\ &- (\varepsilon_1'' - \varepsilon_2'')(\varepsilon_1' + 2\varepsilon_2')\big]\big\}, \end{aligned} \tag{22}$$

$$\begin{aligned} g'' = \varepsilon_2'' + F\big\{&(\varepsilon_2' - 1)\big[(\varepsilon_1'' - \varepsilon_2'')(\varepsilon_1' + 2\varepsilon_2') \\ &- (\varepsilon_1' - \varepsilon_2')(\varepsilon_1'' + 2\varepsilon_2'')\big] + \varepsilon_2''\big[(\varepsilon_1' - \varepsilon_2')(\varepsilon_1' + 2\varepsilon_2') \\ &+ (\varepsilon_1'' - \varepsilon_2'')(\varepsilon_1'' + 2\varepsilon_2'')\big]\big\} \end{aligned} \tag{23}$$

with ε_i' and ε_i'' the real and imaginary parts of the dielectric functions of the core ($i = 1$) and the coat ($i = 2$) including the effect of surplus electrons. For uncharged particles $\varepsilon_i = \bar{\varepsilon}_i$.

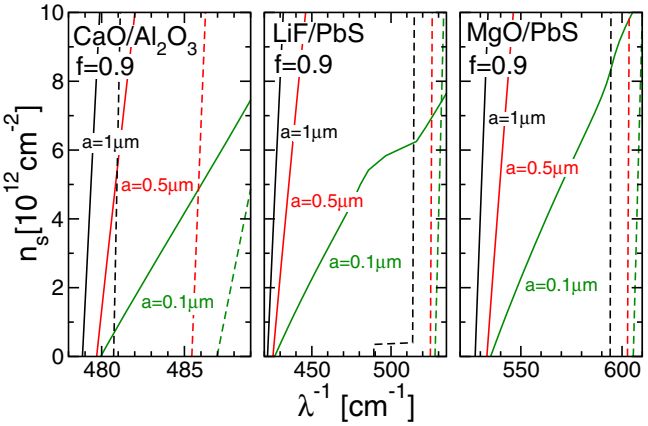

Fig. 5. Position of the extinction maximum due to the anomalous resonance of the core (feature C in Fig. 4) for a CaO/Al_2O_3 (left panel), a LiF/PbS (middle panel), and a MgO/PbS particle (right panel) as a function of surface charge density n_s. The filling factor $f = 0.9$ while the radius a of the particles changes as indicated. Dashed lines give the positions of the anomalous extinction maxima of the corresponding homogeneous core particles with the same radius.

The third row of Figure 4 shows g' and g'' as defined by equations (22) and (23) for a CaO/Al_2O_3 particle with $a = 0.1\ \mu$m. In the vicinity of the features A_2 and B g'' is nearly constant whereas g' crosses zero. The two roots indicated by the dotted vertical lines are the bonding and anti-bonding partners of the mixing doublet found in the electrostatic approximation. In the following we refer to the bonding partner as the anomalous resonance of the coat and to the anti-bonding partner as the shell resonance. Whether or not the latter appears depends on the dielectric functions of the materials as should be obvious from the complicated dependence of g' and g'' on the real and imaginary parts of the dielectric functions of the core and the coat. Not all coated dielectric particles will thus show a shell resonance.

Now we turn to charged coated dielectric particles. In addition to the dielectric functions of the materials the density of surplus electrons is now also an important parameter. It enters the dielectric function of the coat ε_2 via the electric conductivity (11) where n_{a-b} is the volume density of the surplus electrons, that is, the number of surplus electrons divided by the coat volume. Conceptually we found it however more convenient to relate the particle charge to the particle surface. Instead of n_{a-b} we use therefore $n_s = (a^3 - b^3)n_{a-b}/3a^2$ to specify the charge of the particle. The number of elementary charges carried by the particle is then $Z_p = 4\pi a^2 n_s$.

The three dominant features showing up in the extinction of an uncharged coated particle – feature A_2, B, and C – are charge-sensitive. In Figure 5 we depict for three kinds of coated particles on the abscissa the position of the anomalous resonance of the core (feature C) as a function of the surface charge density n_s. The filling factor is fixed to $f = 0.9$ and the radii change as indicated. In comparison to homogeneous particles of the same size consisting only of the core material and having

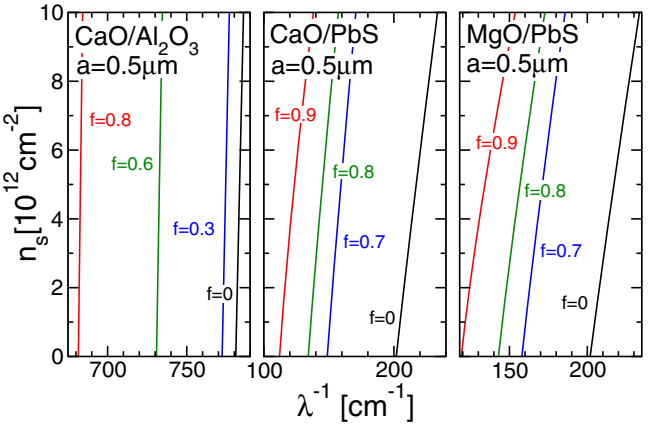

Fig. 6. Position of the extinction maximum due to the anomalous resonance of the coat (feature A_2 in Fig. 4) for a CaO/Al_2O_3 (left panel), a CaO/PbS (middle panel), and a MgO/PbS particle (right panel) as a function of surface charge density n_s. The radius $a = 0.5$ μm while the filling factor f of the particles varies as indicated.

thus no coating (dashed lines) two differences have to be noted: first, the positions of the resonances for the uncharged particles, the base points in Figure 5, are shifted to smaller wave numbers. The red-shift depends also on the filling factor (not shown). It is thus possible to adjust to a certain extent the spectral window where the particle responds most strongly to infrared radiation. Second, the slope of the solid lines in Figure 5 is in general less steep than the slope of the dashed lines. Consider, for instance, a CaO/Al_2O_3 particle with radius $a = 1$ μm. The slope $\Delta n_s/\Delta\lambda^{-1} \approx 11.3 \times 10^{12}$ cm^{-1} compared to $\Delta n_s/\Delta\lambda^{-1} \approx 45 \times 10^{12}$ cm^{-1} found for a homogeneous CaO particle of the same size[1]. Clearly, the coating increases the charge sensitivity of the anomalous resonance of the core by a factor four. For smaller particles the effect of the coating is similar. Reducing the radius to $a = 0.1$ μm leads to $\Delta n_s/\Delta\lambda^{-1} \approx 0.82 \times 10^{12}$ cm^{-1} compared to $\Delta n_s/\Delta\lambda^{-1} \approx 2.3 \times 10^{12}$ cm^{-1} and hence to an increase of the charge sensitivity by a factor three.

Similar charge effects can be found for the anomalous extinction resonance of the coat (feature A_2) which–we recall–is the bonding partner of the doublet predicted by the electrostatic approximation [35]. In Figure 6 we plot the position of this resonance for CaO/Al_2O_3, CaO/PbS, and MgO/PbS particles with fixed radius $a = 0.5$ μm and varying filling factor f. For $n_s = 0$ and $f = 0$ the resonances are at the positions expected for the uncharged homogeneous particles completely made out of the coat material. In accordance with the physical picture emerging from the electrostatic approximation [35] the base points move with increasing f to smaller wave numbers while adding surface charges shifts the resonances irrespective of f and for all material combinations shown in Figure 6 to larger wave numbers. The rate of this shift and thus the charge sensitivity is surprisingly slightly smaller than for homogeneous particles of the same size but made out of the coat material alone ($f = 0$). For instance, for a CaO/Al_2O_3 particle with $a = 0.5$ μm and $f = 0.8$ the slope $\Delta n_s/\Delta\lambda^{-1} \approx 3.7 \times 10^{12}$ cm^{-1} while for a homogeneous Al_2O_3 particle $\Delta n_s/\Delta\lambda^{-1} \approx 2.1 \times 10^{12}$ cm^{-1}.

The resonances we discussed in Figures 5 and 6 can be traced back to the resonances homogeneous core or coat particles would also support. The core-coat structure shifted the position of the resonances of the uncharged particles to smaller wave numbers, added therefore some flexibility in defining the spectral window where the particle optically responds to its charge, and increased (core resonance) or slightly decreased (coat resonance) the charge sensitivity. The charge the particles have to carry is however still high. For a shift of the core resonance on the order of a wave number a particle with radius $a = 0.5$ μm and filling factor $f = 0.9$ has to charge up to $n_s \approx 4.5 \times 10^{12}$ cm^{-2} which is equivalent to 1.4×10^5 elementary charges.

We now turn to the anti-bonding partner of the mixing doublet (feature B), what we call shell resonance. In Figure 7 we plot the extinction efficiency Q_t due to this resonance for a CaO/Al_2O_3 particle with radius $a = 0.3$ μm and filling factor $f = 0.95$ as a function of the wave number and the surface charge density. Also shown is the position of the shell resonance as a function of the particle radius, the filling factor, and the core material. We note two important points which make this resonance particularly attractive for our purpose: first, the shell resonance appears above 800 cm^{-1}, deep in the far-infrared. For the infrared instrumentation this is a great advantage [32]. Second and more importantly, the charge the particle has to carry for a noticeable shift to occur is now one order of magnitude lower compared to the charge it would have to carry to shift by the same amount any one of the anomalous resonances of the core- or coat-type. For a micron-sized particle, for instance, the slope $\Delta n_s/\Delta\lambda^{-1} \approx 3.3 \times 10^{11}$ cm^{-1} and thus roughly a factor 34 smaller than the slope found for the core resonance. To produce therefore a shift of one wave number the particle has to charge up only to $n_s \approx 3.3 \times 10^{11}$ cm^{-2} implying 4×10^4 elementary charges and not 1.4×10^6. As it was the case for the anomalous core resonance, the smaller the particle the smaller the slope and hence the larger the charge-induced shift. For instance, the slope associated with the extinction maximum shown in the left panel of Figure 7 is $\Delta n_s/\Delta\lambda^{-1} \approx 9.2 \times 10^{10}$ cm^{-2}. Hence, the maximum shifts already by one wave number for $Z_p \approx 10^3$, a value which seems to be realistic for a particle with $a = 0.3$ μm.

It is the position of the shell resonance we propose to use as a charge diagnostics because of its charge sensitivity and its high wave number. The former opens the door to measure particle charges in ordinary [9] and not only in highly specialized [33,34] dusty laboratory plasmas while the latter lessens the requirements on the infrared

[1] Note, CaO, LiF, and MgO have negative electron affinity. The boundary conditions for the electromagnetic fields to be used in the calculation of the extinction efficiency for the homogeneous CaO, LiF, and MgO particles are thus not (A.22) and (A.23) but the ones used in [19,20] for particles with negative electron affinity.

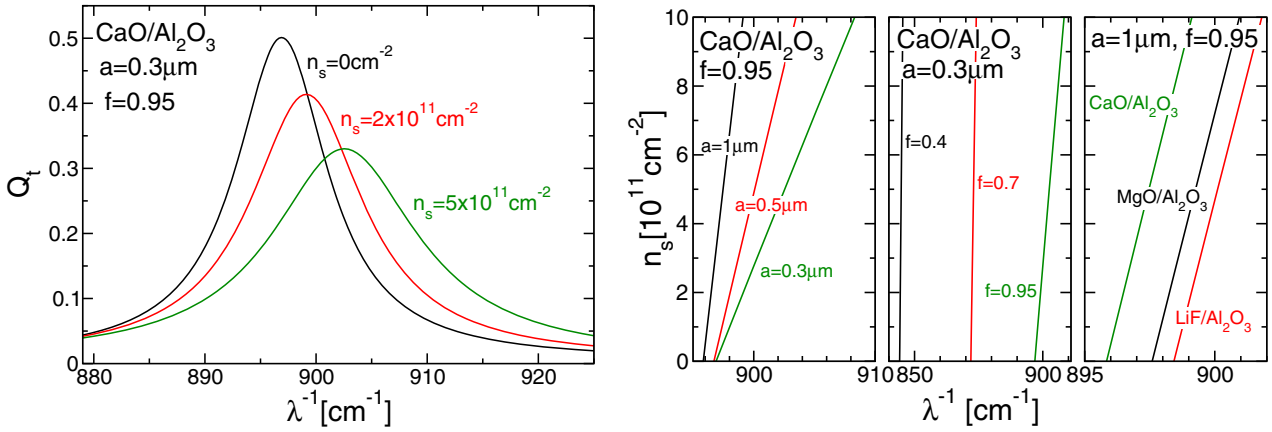

Fig. 7. Left panel: extinction efficiency Q_t due to the shell resonance (feature B in Fig. 4) for a CaO/Al_2O_3 particle as a function of the wave number λ^{-1} and surface charge density n_s. The radius $a = 0.3$ μm and the filling factor $f = 0.95$. Right panel: position of the extinction maximum for fixed filling factor f and varying radius a, for fixed radius and varying filling factor, and for fixed radius and filling factor but varying core material.

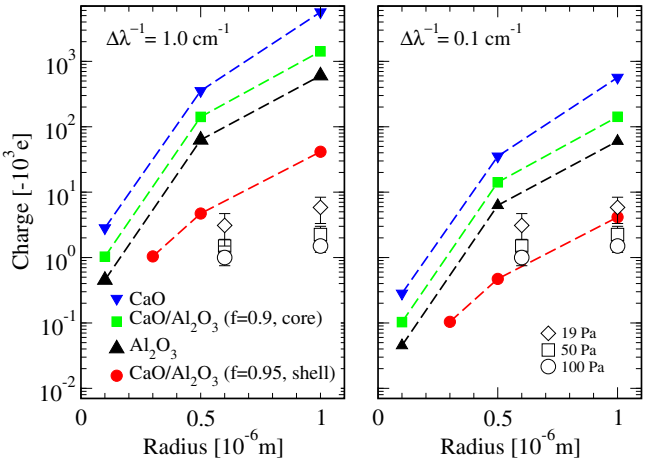

Fig. 8. Particle charge necessary to shift the extinction resonance of the indicated particles by one wave number (left panel) and by one-tenth of a wave number (right panel). Also shown are experimental data with error bars from Khrapak et al. [16] for melamine-formaldehyde particles in a neon discharge at three different gas pressures.

instrumentation [32]. The shell resonance does however not always appear. It shows up only when the dielectric functions of the core and the coat material are such that g' defined in equation (22) has a root and g'' given by equation (23) is rather small. Nevertheless there are a number of material combinations which could be used. Besides CaO/Al_2O_3 particles, MgO/Al_2O_3 and LiF/Al_2O_3 particles support a shell resonance. The charge-induced shift plotted in the far most right panel of Figure 7 is roughly the same for all three material combinations.

To summarize our results we collect in Figure 8 for the CaO-Al_2O_3 material system the charges homogeneous and coated particles of various sizes have to carry to shift the extinction resonance (either core or shell resonance) by one wave number (left panel) or by one-tenth of a wave number (right panel) and compare it to the charges melamine-formaldehyde particles acquire in a neon discharge at three different gas pressures [16]. Comparing the data for the CaO/Al_2O_3 particle with the data for the homogeneous CaO particle shows the increase of the charge sensitivity due to the coating. The plot also shows that a homogeneous Al_2O_3 particle is slightly better than a coated CaO/Al_2O_3 particle if the core resonance is used as a charge diagnostic. If however the shell resonance is used, the coated particle beats the two homogeneous ones by orders of magnitude. It is clearly the best choice. For a high-end interferometer with a resolution of one-tenth of a wave number the shift of the shell resonance should be detectable for particles as large as a micron. Interferometers with a resolution of only one wave number should still be able to measure the charge of particles with a radius of half a micron.

4 Conclusions

We studied the infrared extinction of charged dielectric particles consisting of an inner core with negative and an outer coat with positive electron affinity and identified three charge-sensitive features in the extinction spectrum. Besides the maxima in the extinction due to the anomalous resonances of the core and the coat material we found a third extinction maximum due to the core-coat structure at wave numbers above the anomalous resonance of the coat. In the electrostatic approximation this resonance, which we call shell resonance, can be attributed to the anti-bonding mixing of the anomalous resonance of a hypothetical particle consisting only of the coat material and having the radius of the particle under consideration and a mode due to the cavity which arises due to replacing the central portion of the particle by another material. The positions of the three types of extinction maxima depend on the particle charge showing that in principle the charge could be determined optically by recording the charge-induced shift of any of these extinction maxima.

In order to determine the particle charge optically specially designed particles should be used to enhance the effect as much as possible. Using a core with negative electron affinity prevents electrons from entering the core and hence forces the surplus electrons to pile up in the coat region. Controlling the location of the surplus electrons is only the first step. In a second step the coat has to be chosen such that a strong shell resonance appears in a spectral region easy to handle. For a PbS coat the shell resonance is in the mid-infrared while for an Al_2O_3 coat it appears in the far-infrared. Since we expect the latter easier to handle we focused on particles with an Al_2O_3 coating although a PbS coating with its smaller electron effective mass would lead to an improved charge sensitivity.

Using coated particles with tailor-made electric and optical properties adds flexibility to the proposed optical charge measurement and enhances the sensitivity of the approach. Infrared interferometers with a resolution on the order of one wave number should be able to detect the shift of the extinction maximum of the charged particle compared to the uncharged one up to particle radii of half a micron. With an high-end interferometer, having a resolution better than 1/10 of a wave number, it would be even possible to determine the shift for micron-sized particles. From the results shown in Figure 8 we would expect particles with a radius of 0.1–0.5 μm to be the best candidates for an optical charge measurement in ordinary dusty laboratory plasmas. Increasing the particle charge due to a judicious choice of the plasma conditions would of course lessen the requirements on the particle size and/or the infrared spectroscopy.

After an experimental proof of principle, the greatest challenge will be the calibration of the approach. This has to be achieved by an interplay between theory and experiment, possibly using particles confined in a trap [50], and consists – after choosing a particular type of particle – of two main steps. First, the base point of the line $n_s(\lambda^{-1})$ has to be fixed experimentally. It depends on the morphology and the geometry of the particle. In particular the latter could be an issue. So far we assumed the particles to have perfect spherical shape. In reality this is of course not the case. But only experiments can tell to what extent the non-spherical shape affects the Mie signal. If necessary we could within the electro-static approximation take the shape of real dust particles into account. Averaging over a size distribution would be no problem. Second, the charge-induced shift has to be measured and compared with the theoretical predictions. The shift depends on the conductivity of the surplus electrons. At the moment we calculate the conductivity within a planar bulk model sufficient for particles with radii larger than 0.1 μm and filling factors less than 0.95 where curvature and/or quantum confinement effects can be ignored. We could include these effects if the need arises. We also made a selection with respect to the scattering process limiting the conductivity taking into account only electron-phonon scattering which we expect to be the dominant process. High-precision measurements of the shift may reveal that sub-dominant scattering processes contribute as well. Within the memory function formalism we could include them straightforwardly. To make further progress, that is, to make the optical measurement of the charge of submicron- and micron-sized particles in a plasma a reality, experiments have thus to come in and guide the theoretical calculations of the extinction efficiency.

This work was supported by the Deutsche Forschungsgemeinschaft through the Transregional Collaborative Research Center SFB/TRR24. Discussions with J. Röpcke and F. Greiner are greatly acknowledged.

Appendix: Calculation of the extinction efficiency

To make our presentation self-contained we sketch in this Appendix the main steps of the calculation of the Mie scattering coefficients for a coated spherical particle. Aden and Kerker [36] were the first who studied the scattering of an electromagnetic plane wave by two concentric spheres separating three spatial regions with different dielectric properties. The calculation can be also found in the textbook by Bohren and Huffman [23].

The starting point is the general solution of the source-free Fourier-transformed Maxwell equations [23],

$$\nabla \cdot (\varepsilon \boldsymbol{E}) = 0, \quad \nabla \times \boldsymbol{E} = i\frac{\omega\mu}{c}\boldsymbol{H}, \tag{A.1}$$

$$\nabla \cdot \boldsymbol{H} = 0, \quad \nabla \times \boldsymbol{H} = -i\frac{\omega\varepsilon}{c}\boldsymbol{E}, \tag{A.2}$$

where ε is the dielectric function, μ is the magnetic permeability, and c is the speed of light, in terms of vector spherical harmonics. In the notation of Bohren and Huffman [23],

$$\boldsymbol{E} = \sum_{n=1}^{\infty} \left(A_n \boldsymbol{N}_n + B_n \boldsymbol{M}_n\right), \tag{A.3}$$

$$\boldsymbol{H} = \frac{kc}{i\omega\mu} \sum_{n=1}^{\infty} \left(A_n \boldsymbol{M}_n + B_n \boldsymbol{N}_n\right) \tag{A.4}$$

with

$$\boldsymbol{M} = \nabla \times \boldsymbol{r}\psi \quad \text{and} \quad \boldsymbol{N} = k^{-1}\nabla \times \boldsymbol{M} \tag{A.5}$$

the vector spherical harmonics defined by the function ψ which satisfies the scalar wave equation,

$$\nabla^2\psi + k^2\psi = 0 \tag{A.6}$$

with $k^2 = \omega^2\varepsilon\mu/c^2$.

Using spherical coordinates with the propagation direction of the incident plane wave defining the z-axis and the center of the particle defining the origin of the coordinate system, the solution of (A.6) is either

$$\psi_{omn}(\phi, \theta, r) = \sin(m\phi) P_n^m(\cos\theta) z_n(kr) \tag{A.7}$$

or

$$\psi_{emn}(\phi,\theta,r) = \cos(m\phi)P_n^m(\cos\theta)z_n(kr) \tag{A.8}$$

with $P_n^m(x)$ associated Legendre polynomials ($n = m, m+1,\ldots$), $z_n(x)$ any kind of spherical Bessel function [48], and subscripts e and o denoting, respectively, even and odd symmetry with respect to the azimuth angle ϕ.

To proceed the expansions (A.3) and (A.4) have to be specified to the particular regions: region 1 (core), region 2 (coat), and region 3 (outer space). In the outer space, the electromagnetic field consists of an incident plane wave,

$$\boldsymbol{E}_{\rm in} = \sum_{n=1}^{\infty} E_n \left(\boldsymbol{M}_{o1n}^{(1)} - i\boldsymbol{N}_{e1n}^{(1)}\right), \tag{A.9}$$

$$\boldsymbol{H}_{\rm in} = -\frac{kc}{\omega\mu}\sum_{n=1}^{\infty} E_n \left(\boldsymbol{M}_{e1n}^{(1)} + i\boldsymbol{N}_{o1n}^{(1)}\right) \tag{A.10}$$

with expansion coefficients

$$E_n = i^n E_0 \frac{2n+1}{n(n+1)}, \tag{A.11}$$

where E_0 is the strength of the electric field of the incident wave, and the scattered fields

$$\boldsymbol{E}_s = \sum_{n=1}^{\infty} E_n \left(ia_n\boldsymbol{N}_{e1n}^{(3)} - b_n\boldsymbol{M}_{o1n}^{(3)}\right), \tag{A.12}$$

$$\boldsymbol{H}_s = \frac{kc}{\omega\mu}\sum_{n=1}^{\infty} E_n \left(ib_n\boldsymbol{N}_{o1n}^{(3)} + a_n\boldsymbol{M}_{e1n}^{(3)}\right). \tag{A.13}$$

The superscripts indicate which kind of Bessel function has to be used in the definition of the vector spherical harmonics (A.5). The superscripts (1) and (2) stand respectively for spherical Bessel functions of the first and second kind, while the superscript (3) signals a Bessel function of the third kind, that is, a Hankel function [48]. The field in the coat region is given by:

$$\boldsymbol{E}_2 = \sum_{n=1}^{\infty} E_n \Big(f_n\boldsymbol{M}_{o1n}^{(1)} - ig_n\boldsymbol{N}_{e1n}^{(1)} \tag{A.14}$$

$$+ v_n\boldsymbol{M}_{o1n}^{(2)} - iw_n\boldsymbol{N}_{e1n}^{(2)}\Big), \tag{A.15}$$

$$\boldsymbol{H}_2 = -\frac{k_2c}{\omega\mu_2}\sum_{n=1}^{\infty} E_n \Big(g_n\boldsymbol{M}_{e1n}^{(1)} + if_n\boldsymbol{N}_{o1n}^{(1)} \tag{A.16}$$

$$+ w_n\boldsymbol{M}_{e1n}^{(2)} + iv_n\boldsymbol{N}_{o1n}^{(2)}\Big) \tag{A.17}$$

while in the core region it becomes

$$\boldsymbol{E}_1 = \sum_{n=1}^{\infty} E_n \left(c_n\boldsymbol{M}_{o1n}^{(1)} - id_n\boldsymbol{N}_{e1n}^{(1)}\right), \tag{A.18}$$

$$\boldsymbol{H}_1 = -\frac{k_1c}{\omega\mu_1}\sum_{n=1}^{\infty} E_n \left(d_n\boldsymbol{M}_{e1n}^{(1)} + ic_n\boldsymbol{N}_{o1n}^{(1)}\right). \tag{A.19}$$

Using the orthogonality of the vector spherical harmonics [22,23], the eight expansion coefficients a_n, b_n, c_n, d_n, f_n, g_n, v_n and w_n can be straightforwardly calculated from the boundary conditions. At $r = b$, the core-coat boundary,

$$\left(\boldsymbol{E}_2 - \boldsymbol{E}_1\right) \times \boldsymbol{r} = 0, \tag{A.20}$$

$$\left(\boldsymbol{H}_2 - \boldsymbol{H}_1\right) \times \boldsymbol{r} = 0, \tag{A.21}$$

while at $r = a$, that is, at the coat-outer space boundary

$$\left(\boldsymbol{E}_s + \boldsymbol{E}_{\rm in} - \boldsymbol{E}_2\right) \times \boldsymbol{r} = 0, \tag{A.22}$$

$$\left(\boldsymbol{H}_s - \boldsymbol{H}_{\rm in} - \boldsymbol{H}_2\right) \times \boldsymbol{r} = 0. \tag{A.23}$$

The coefficients a_n and b_n required for the calculation of the extinction efficiency (1) turn then out to be given by equations (2)–(7) of the main text [36,37].

References

1. O. Ishihara, J. Phys. D **40**, R121 (2007)
2. V.E. Fortov, A.V. Ivlev, S.A. Khrapak, A.G. Khrapak, G.E. Morfill, Phys. Rep. **421**, 1 (2005)
3. I. Mann, Adv. Space Res. **41**, 160 (2008)
4. L. Spitzer, *Processes in the Interstellar Medium* (Wiley, 1982)
5. E. Gruen, G. Morfill, D.A. Mendis, in *Planetary Rings*, edited by R. Greenberg, A. Brahic (University of Arizona Press, Tuscon, 1984), p. 275
6. M. Friedrich, M. Rapp, Surv. Geophys. **30**, 525 (2009)
7. C. Hollenstein, Plasma Phys. Control. Fusion **42**, R93 (2000)
8. F. Galli, U.R. Kortshagen, IEEE Trans. Plasma Sci. **38**, 803 (2010)
9. A. Piel, A. Melzer, Plasma Phys. Control. Fusion **44**, R1 (2002)
10. B. Walch, M. Horányi, S. Robertson, Phys. Rev. Lett. **75**, 838 (1995)
11. A. Homann, A. Melzer, S. Peters, A. Piel, Phys. Rev. E **56**, 7138 (1997)
12. E.B. Tomme, D.A. Law, B.M. Annaratone, J.E. Allen, Phys. Rev. Lett. **85**, 2518 (2000)
13. A. Melzer, Phys. Rev. E **67**, 016411 (2003)
14. V.E. Fortov, O.F. Petrov, A.D. Usachev, A.V. Zobnin, Phys. Rev. E **70**, 046415 (2004)
15. H. Kersten, H. Deutsch, G.M.W. Kroesen, Int. J. Mass Spectrom. **233**, 51 (2004)
16. S.A. Khrapak, S.V. Ratynskaia, A.V. Zobnin, A.D. Usachev, V.V. Yaroshenko, M.H. Thoma, M. Kretschmer, H. Hoefner, G.E. Morfill, O.F. Petrov, V.E. Fortov, Phys. Rev. E **72**, 016406 (2005)
17. J. Carstensen, F. Greiner, A. Piel, Phys. Plasmas **17**, 083703 (2010)
18. J. Carstensen, H. Jung, F. Greiner, A. Piel, Phys. Plasmas **18**, 033701 (2011)
19. R.L. Heinisch, F.X. Bronold, H. Fehske, Phys. Rev. E **88**, 023109 (2013)
20. R.L. Heinisch, F.X. Bronold, H. Fehske, Phys. Rev. Lett. **109**, 243903 (2012)
21. G. Mie, Ann. Phys. **25**, 377 (1908)

22. J.A. Stratton, *Electromagnetic Theory* (McGraw-Hill, 1941)
23. C.F. Bohren, D.R. Huffman, *Absorption and Scattering of Light by Small Particles* (Wiley, 1983)
24. C.F. Bohren, A.J. Hunt, Can. J. Phys. **55**, 1930 (1977)
25. J. Rostalski, M. Quinten, Colloid Polym. Sci. **274**, 648 (1996)
26. J. Klačka, M. Kocifaj, J. Quant. Spectrosc. Radiat. Transfer **106**, 170 (2007)
27. J. Klačka, M. Kocifaj, Prog. Electromagn. Res. **109**, 17 (2010)
28. A. Heifetz, H.T. Chien, S. Liao, N. Gopalsami, A.C. Raptis, J. Quant. Spectrosc. Radiat. Transfer **111**, 2550 (2010)
29. M. Rosenberg, IEEE Trans. Plasma Sci. **40**, 1229 (2012)
30. M.I. Tribelsky, B.S. Luk'yanchuk, Phys. Rev. Lett. **97**, 263902 (2006)
31. M.I. Tribelsky, Europhys. Lett. **94**, 14004 (2011)
32. J. Röpcke, J. Lombardi, G. Rousseau, P.B. Davies, Plasma Sources Sci. Technol. **15**, S148 (2006)
33. A.V. Filippov, M.N. Vasilev, A.V. Gavrikov, A.F. Pal, O.F. Petrov, A.N. Starostin, V.E. Fortov, J. Exp. Theor. Phys. Lett. **86**, 14 (2007)
34. V.E. Fortov, A.V. Gavrikov, O.F. Petrov, V.S. Sidorov, M.N. Vasiliev, N.A. Vorona, Europhys. Lett. **94**, 55001 (2011)
35. T.C. Preston, R. Signorell, Proc. Natl. Acad. Sci. USA **108**, 5532 (2012)
36. A.L. Aden, M. Kerker, J. Appl. Phys. **22**, 1214 (1951)
37. E. Thiessen, Master thesis, Universität Greifswald, 2013
38. A.M. Hofmeister, E. Keppel, A.K. Speck, Mon. Not. R. Astron. Soc. **345**, 16 (2003)
39. J.R. Jasperse, A. Kahan, J.N. Plendl, S.S. Mitra, Phys. Rev. **146**, 526 (1966)
40. R. Geick, Phys. Lett. **10**, 51 (1964)
41. E.D. Palik, *Handbook of Optical Constants of Solids* (Academic, 1985)
42. A.S. Barker, Phys. Rev. **132**, 1474 (1963)
43. A.K. Walton, T.S. Moss, B. Ellis, Proc. Phys. Soc. Lond. **79**, 1065 (1962)
44. T.V. Perevalov, A.V. Shaposhnikov, V.A. Gritsenko, H. Wong, J.H. Hund, C.W. Kim, J. Exp. Theor. Phys. Lett. **85**, 165 (1979)
45. R.L. Heinisch, F.X. Bronold, H. Fehske, Phys. Rev. B **85**, 075323 (2012)
46. F.X. Bronold, H. Deutsch, H. Fehske, Eur. Phys. J. D **54**, 519 (2009)
47. W. Götze, P. Wölfle, Phys. Rev. B **6**, 1226 (1972)
48. *Handbook of Mathematical Functions*, edited by M. Abramowitz, I.A. Stegun (Dover Publications, Inc., New York, 1973)
49. H.R. Maurer, H. Kersten, J. Phys. D **44**, 174029 (2011)
50. M. Beránek, I. Čermák, Z. Němeček, J. Šafránková, M. Jeřáb, J. Pavlů, Rev. Sci. Instrum. **83**, 115109 (2012)